Spallation of gold by 100–300 MeV pions

S. B. Kaufman and E. P. Steinberg
Chemistry Division, Argonne National Laboratory, Argonne, Illinois 60439

G. W. Butler
Los Alamos Scientific Laboratory, Los Alamos, New Mexico 87545

(Received 11 June 1979)

Cross sections of radioactive products resulting from the interactions of 100-, 180-, and 300-MeV π^+ and π^- mesons with gold have been determined by analysis of the γ-ray spectra of bombarded target foils. More than 30 nuclides were identified between mass numbers 167 and 196. The results indicate the following. (1) The most probable charge for a given mass lies several charge units to the neutron-poor side of the beta-stability line. (2) The average cross-section ratios $\sigma(\pi^-)/\sigma(\pi^+)$ for all measured nuclides are 1.34, 1.23, and 1.05 at 100, 180, and 300 MeV, respectively. At a given energy there is no systematic variation of the ratio with nuclide mass number. These results are what is expected from Coulomb effects, with no indication of an isospin effect due to the large T_Z of the target. (3) The influence of the (3,3) resonance is apparent in the total reaction cross section. (4) The average excitation energy transferred to the nucleus is similar for π^+ and π^- induced reactions and increases with increasing pion kinetic energy. Comparisons of the data with intranuclear cascade-evaporation calculations indicate that the latter predict less pion absorption than actually occurs.

[NUCLEAR REACTIONS ^{197}Au ($\pi^{\pm}$, spallation), $E = 100$–300 MeV; measured σ for products $167 \leq A \leq 196$; estimated total reaction cross sections.]

I. INTRODUCTION

The study of multinucleon removal from the interactions of energetic pions in the resonance region (i.e., up to ~300 MeV) with complex nuclei has been the subject of a number of recent experiments. The distributions of final nuclei have been determined by both prompt γ-ray measurements[1-13] and by activation measurements.[13-16] The general features of the product yield distributions are as follows: (a) The maximum yields tend to lie along the line of beta stability, and appear to be determined largely by evaporation processes. (b) The amount of energy deposited in the nucleus, as measured by the average number of nucleons removed, is nearly independent of pion charge and energy, from stopped pions to energies of ~220 MeV. (c) Comparisons of pion- and proton-induced yields show the importance of pion absorption in transferring energy to the nucleus.

All of the previous studies have been carried out using light- to medium-weight targets, and one might expect substantial differences in the experimental results with a heavy target having a large N/Z ratio. For example, the evaporation of charged particles will be strongly suppressed by the large Coulomb barrier, and thus the nuclides of maximum yield will tend to be neutron deficient, rather than beta stable. This is a disadvantage in a prompt γ-ray study, since the primary products will tend to have little-known level schemes. On the other hand, it is an advantage in an activation experiment, since most products will be radioactive, thus permitting a major fraction of the yield to be studied.

One might also expect to observe substantial differences in cross sections for incident π^- and π^+ mesons due both to the nuclear Coulomb field and to isospin effects. The former arises because an incident π^- is attracted by the nucleus while a π^+ is repelled, thus increasing the reaction cross section of the former over that of the latter. Isospin effects can occur because of the large N/Z ratio of a heavy nucleus. For example, in the region of the (3, 3) resonance, the scattering cross section of π^- by neutrons is about three times that for protons, while the converse is true for π^+. Thus, nuclides formed as a result of scattering might have larger cross sections for incident π^- than for π^+. On the other hand, the neutron excess nature of the target would enhance π^+ absorption over π^- absorption, leading to a lower $\sigma(\pi^-)/\sigma(\pi^+)$ ratio for nuclides formed primarily by pion absorption.

We report here the results of activation measurements of gold targets with both negative and positive pions of kinetic energies 100, 180, and 300 MeV. A Ge(Li) detector was used to measure the γ-ray spectrum of the target following the irradiation, and cross sections for a number of radionuclides were determined. The cross sec-

tions for missing nuclides were estimated by interpolation, and thus the total reaction cross section could be calculated. Detailed comparisons will be made between the experimental data and the results of intranuclear cascade-evaporation calculations. Comparisons between these data with energetic (100–300 MeV) pions and recent measurements[17-22] of stopped pions in heavy targets will also be made.

The formation cross sections for the nuclide ^{196}Au have been published previously[23] and the significance of the $(\pi^{\pm}, \pi N)$ cross sections and cross section ratios discussed in that publication.

II. EXPERIMENTAL

The experiments were performed using the beams of the P^3 channel[24] of the Clinton P. Anderson Meson Physics Facility (LAMPF). The beam was tuned to provide energies of 100, 180, and 300 MeV for these experiments, with a momentum spread of 6%. Protons were removed from the π^+ beams by differential energy degradation; at 300 MeV the proton contamination was less than 1%, and was negligible at lower energies. The dimensions of the beam at the target position were smaller than the target size, which was 4 $\times$ 4 cm, as established by exposure of Polaroid film prior to each irradiation.

The irradiation conditions are summarized in Table I, which gives the average pion flux, the duration of the bombardment, target thickness, and the beam monitor cross section. The targets consisted of one or more aluminum monitor foils upstream of the gold target and separated from it by Mylar guard foils. In order to learn if secondary reactions of particles produced in the target were contributing to any of the products, two irradiations with 180 MeV π^+ mesons were done with target thicknesses which differed by a factor of four, as shown in Table I. The measured cross sections for these duplicate runs showed no systematic differences. In particular, the cross section ratios between products within a few mass numbers from the target and those far removed in mass, which would be expected to be sensitive to secondary effects, were identical to within 1%.

Variations of beam intensity during the irradiation were measured using a scintillator positioned off the beam axis near the target, and recorded with a strip chart; corrections for such variation were made in calculating cross sections. Following the irradiation, the monitor and target foils were separated and their γ-ray spectra measured with calibrated Ge(Li) spectrometers. The 1368.5-keV γ-ray of ^{24}Na was measured in the monitor foil, and the total number of pions incident was calculated from the disintegration rate extrapolated to the end-of-bombardment (D^{EOB}) and the formation cross section of ^{24}Na from aluminum. The values used[25] for these monitor cross sections are given in Table I; there is an uncertainty of about 10% in these cross sections.

The gold target was counted initially at Los Alamos in order to detect short-lived nuclides, and was then transferred to Argonne National Laboratory, where the counting continued for several months. The Ge(Li) spectrometers used were calibrated using standard mixed sources obtained from the National Bureau of Standards. The energy resolution of the detectors was 2.0 keV (FWHM) at 1332 keV. The spectra, recorded on magnetic tape, were analyzed using two computer programs, GAMANAL[26] and SAMPO.[27] Peaks in the spectra were identified and assigned to specific nuclides on the basis of energy and half-life. The decay characteristics of the nuclides identified in this work are given in Table II. The γ-ray abundances were obtained from the Nuclear Data Sheets[28] or from recent compilations.[29,30] For two of the nuclides in Table II, ^{191}Au and ^{186}Pt, absolute γ-ray intensities are unknown, and thus only relative cross sections could be determined.

In calculating the disintegration rate of a nuclide

TABLE I. Pion irradiation conditions.

Beam energy (MeV) and charge	Average flux (sec^{-1})	Duration (h)	Target thickness ($\mathrm{mg/cm}^2$) Au	Al	Monitor cross section (mb)
$100\pi^+$	1.86×10^7	5.63	188.5	52.2	12.3
$100\pi^-$	9.23×10^6	6.00	186.8	52.5	22.0
$180\pi^+$	5.02×10^7	5.60	193.4	51.6	21.2
$180\pi^+$	7.06×10^7	13.34	55.4	13.9	21.2
$180\pi^-$	1.59×10^7	4.98	190.9	52.5	24.0
$300\pi^+$	1.47×10^8	4.69	95.4	26.0	14.3
$300\pi^-$	5.57×10^7	7.18	193.4	51.9	15.9

TABLE II. Decay properties of nuclides observed.

Nuclide	$T_{1/2}$	Observed γ rays (keV)	Abundances
^{196}Au	6.18 day	333.0; 355.7	0.238; 0.88
^{196}Au^{m}	9.7 h	147.8	0.45
^{194}Au	39.5 h	293.6; 328.5	0.104; 0.591
^{193}Hg^{m}	11.1 h	258.0	0.72
^{193}Au	17.7 h	255.6	0.058
^{192}Hg	4.9 h	274.8	0.42
^{192}Au	5.03 h	316.5	0.48
^{192}Ir	74.0 day	316.5	0.831
^{191}Au	3.18 h	283.9	
^{191}Pt	2.8 d	409.4; 538.9	0.080; 0.137
^{190}Ir	12.1 d	557.8; 605.3	0.273; 0.382
^{189}Ir	13.3 d	244.8	0.067
^{188}Pt	10.2 d	187.6; 195.1	0.19; 0.18
^{188}Ir	41.5 h	155.0	0.34
^{186}Pt	2.0 h	689.2	
^{186}Ir^{m}	15.8 h	296.8	0.64
^{185}Ir	14.0 h	254.3	0.14
^{185}Os	93.6 day	646.1	0.813
^{184}Ir	3.02 h	264.0	0.675
^{183}Os	14.0 h	381.8	0.78
^{183}Os^{m}	9.1 h	1102.0; 1108.0	0.50; 0.23
^{183}Re	70 day	162.3	0.26
^{182}Os	22.0 h	180.2	0.37
^{181}Re	20 h	365.5	0.564
^{177}Ta	56.6 h	112.9	0.072
^{176}Ta	8.08 h	1159.3	0.24
^{175}Ta	10.5 h	207.4	0.135
^{175}Hf	70 day	343.4	0.85
^{174}Ta	1.2 h	206.5	0.64
^{173}Hf	24.0 h	123.6	0.828
^{171}Lu	8.22 day	667.3; 739.7	0.12; 0.48
^{169}Lu	34.1 h	191.3; 960.3	0.224; 0.237
^{167}Tm	9.25 day	207.9	0.43

from the observed count rate of a γ ray, a correction was made for the coincidence summing of the γ ray with other γ rays or x rays in the decay of that nuclide. This was necessary because of the close geometry in which the foils were counted, which in turn was necessitated by the low activity levels of the targets. Such corrections were determined empirically whenever possible with more active samples from other (proton) bombardments by counting the sample at varying distances from the detector. In other cases, estimates for the correction were made from a knowledge of the counting efficiency of the detectors as a function of γ-ray energy and the decay scheme of the nuclide.[31]

An important consideration in calculating cross sections from values of the disintegration rate at the end of bombardment (D^{EOB}) is the extent to which a nuclide is formed independently or as the decay product of other nuclides. As will be discussed below, most of the nuclides observed in this work fall in the latter category, i.e., they are formed almost entirely by the decay of short-lived parents. In general, if the independent formation cross sections of parent and daughter nuclides are σ_1 and σ_2, respectively, the observed disintegration rate of the daughter nuclide as a function of time after the end of bombardment is

$$D_2(t) = \left(D_2^{\mathrm{EOB}} + \frac{\lambda_2}{\lambda_1 - \lambda_2} D_1^{\mathrm{EOB}}\right) e^{-\lambda_2 t} - D_1^{\mathrm{EOB}} \frac{\lambda_2}{\lambda_1 - \lambda_2} e^{-\lambda_1 t}, \quad (1)$$

where

$$D_1^{\mathrm{EOB}} = I\sigma_1 N(1 - e^{-\lambda_1 T}) \quad (2)$$

and

$$D_2^{\mathrm{EOB}} = IN\left[\sigma_2(1 - e^{-\lambda_2 T}) + \sigma_1\left(1 - e^{-\lambda_2 T} + \frac{\lambda_2}{\lambda_1 - \lambda_2}(e^{-\lambda_1 T} - e^{-\lambda_2 T})\right)\right]. \quad (3)$$

In Eqs. (1)–(3), I is the beam intensity during an irradiation of length T, N the target thickness in atoms /cm^2, and λ_1 and λ_2 the decay constants of parent and daughter nuclides. For most nuclides observed here, $\sigma_2 = 0$ and the observation time is after essentially all of the parent has decayed, so only the contribution of the first term in Eq. (1) is observed. In that case

$$D_2(t) = I\sigma_1 N(1 - e^{-\lambda_2 T})\left(\frac{\lambda_1}{\lambda_1 - \lambda_2}\right) e^{-\lambda_2 t}. \quad (4)$$

The cross section for production of the parent (σ_1) can then be calculated from Eq. (4). If the parent itself is not formed directly but only from the decay of a still shorter-lived isobar, the analogous equations are much more complex. Since we have very little knowledge about the fractional independent isobaric yields, which would be necessary to treat such a case, we have considered only the immediate parent to the observed nuclide and used Eq. (4). Thus, for example, in the case of 1.2-h ^{174}Ta we assume that its parent, 29-min ^{174}W, was the isobar formed directly, and ignore any contribution from the grandparent, 2.1-min ^{174}Re. When the grandparent's half-life is much shorter than the parent's, as it is in most cases, only a small uncertainty results. Thus, all cumulative cross sections reported in Tables III–V refer to the parent of the listed (observed) nuclide.

If measurements are made soon enough after the end of bombardment to observe both the growth and decay of the daughter, both σ_1 and σ_2 can be

TABLE III. Cross sections from interactions of 100-MeV $\pi^{\pm}$ mesons with ^{197}Au. Independent yields are indicated by (I); others are cumulative. Relative cross sections are indicated by (R). Errors refer to counting statistics only.

Nuclide	$\sigma(\pi^-)$ (mb)	$\sigma(\pi^+)$ (mb)	$\sigma(\pi^-)/\sigma(\pi^+)$
^{196}Au (I)	130 ± 2	68 ± 1	1.91 ± 0.04
^{196}Au^m (I)	6.9 ± 1.4	3.6 ± 0.7	1.92 ± 0.54
^{194}Au (I)	118 ± 2	76 ± 1	1.55 ± 0.03
^{193}Hg^m (I)	<1	17 ± 2	<0.06
^{192}Hg (I)	<2	32 ± 2	<0.06
^{192}Au (I)	114 ±12	65 ±20	1.75 ± 0.57
^{191}Au	8.0 ± 1.4 (R)	7.6 ± 0.9 (R)	1.05 ± 0.22
^{191}Pt	149 ± 8	98 ± 3	1.52 ± 0.09
^{190}Ir (I)	20 ± 2	4.2 ± 1.0	4.8 ±1.2
^{189}Ir	117 ±10	90 ± 5	1.30 ± 0.13
^{188}Pt	84 ± 4	110 ± 6	0.76 ± 0.06
^{188}Ir (I)	45 ±10	6 ± 3	3.3 ±1.8
^{186}Pt	44 ± 2 (R)	83 ± 4 (R)	0.53 ± 0.04
^{186}Ir^m	101 ±10	69 ± 8	1.46 ± 0.22
^{185}Ir	141 ±10	111 ± 6	1.27 ± 0.11
^{185}Os	145 ± 4	114 ± 3	1.27 ± 0.05
^{184}Ir	98 ± 5	99 ± 4	0.99 ± 0.06
^{183}Os	64 ±12	45 ± 9	1.42 ± 0.39
^{183}Os^m	65 ± 4	60 ± 3	1.08 ± 0.09
^{183}Re	123 ± 5	80 ± 3	1.54 ± 0.09
^{182}Os	82 ± 4	60 ± 3	1.37 ± 0.10
^{181}Re	84 ± 4	61 ± 3	1.37 ± 0.10
^{175}Hf	7.6 ± 1.5	6.6 ± 0.7	1.15 ± 0.26
^{167}Tm	3.4 ± 0.9	1.70 ± 0.35	2.0 ±0.7
σ_{obs}	1421 ±25	1058 ±25	$\sigma^-_{obs}/\sigma^+_{obs}$ = 1.34
$\langle \Delta A \rangle$	9.06	9.30	

calculated from Eq. (1). This was possible for four isobaric pairs: 4.9 h ^{192}Hg → 5.03 h ^{192}Au, 10.2 d ^{188}Pt → 41.5 h ^{188}Ir, 2.3 h ^{176}W → 8.08 h ^{176}Ta, and 3.65 h ^{173}Ta → 24.0 h ^{173}Hf. These four isobaric pairs offer interesting contrasts. For the latter two pairs, analysis of the decay curves established that σ_2 was small, and in all cases consistent with $\sigma_2 = 0$ within experimental error. Accordingly we conclude that the nuclides ^{176}Ta and ^{173}Hf are formed entirely by the decay of parent nuclides. In the case of the $A = 188$ isobars, σ_2 for ^{188}Ir was found to be greater than zero for all bombardments, substantially so for π^- and smaller for π^+. In the case of the $A = 192$ isobars, it was found that the 316.5-keV γ ray of ^{192}Au followed an exponential decay with a 5-h half-life in the targets irradiated by π^- mesons, and that no 274.8-keV γ ray corresponding to ^{192}Hg was observed. This is expected, since it is impossible to form Hg isotopes from Au with π^- mesons, except by an exotic reaction such as $(\pi^-, 2\pi^- xn)$.

In contrast, the γ ray of ^{192}Hg was observed in the targets irradiated with π^+ mesons, and the ^{192}Au γ-ray decayed with an apparent half-life of ~8 h, corresponding to the mixed growth and decay curve of parent and daughter.

The absolute abundance of the 316.5-keV γ-ray in the decay of ^{192}Au was not known. However, the growth and decay curve for the 316.5 keV γ-ray could be analyzed with rather large errors to yield values of A_1^{EOB} and A_2^{EOB}, the activities of the parent and daughter at $t = 0$. By comparison of the value of A_1^{EOB} with the value of D_1^{EOB} obtained from the measurements of the 274.8-keV γ ray of ^{192}Hg, the absolute abundance of the 316.5-keV γ ray was determined to be 0.48 ± 0.06 γ rays per ^{192}Au decay.

Most of the nuclides observed represent the cumulative yields of their isobaric precursors. The exceptions are the five nuclides which are shielded by stable or long-lived parents, namely ^{196}Au, ^{194}Au, ^{192}Ir, ^{190}Ir, and ^{188}Ir. In addition, the other isotopes of Au formed in the π^- irradiations are independent, since Hg isotopes are not formed. The isomeric state of ^{196}Au^m decays entirely to the ground state, so the ground state cross section includes that of the isomer.

Several other isomers are observed, which represent only a partial yield at that mass number, such as ^{193}Hg^m and ^{186}Ir^m. Moreover, the

TABLE IV. Cross sections from interactions of 180-MeV $\pi^{\pm}$ mesons with ^{197}Au. Independent yields are indicated by (I); others are cumulative. Relative cross sections are indicated by (R). Errors refer to counting statistics only.

Nuclide	$\sigma(\pi^-)$ (mb)	$\sigma(\pi^+)$ (mb)	$\sigma(\pi^-)/\sigma(\pi^+)$
^{196}Au (I)	181 ± 5	79 ± 1.6	2.29 ± 0.08
^{196}Au^m (I)	4.8 ± 1.0	5.2 ± 1.0	0.92 ± 0.26
^{194}Au (I)	107 ± 3	74 ± 2	1.45 ± 0.06
^{193}Hg^m (I)	<1	11.5 ± 1.5	<0.09
^{193}Au	83 ± 9	74 ± 8	1.12 ± 0.18
^{192}Hg (I)	<2	27.5 ± 2	<0.07
^{192}Au (I)	119 ± 12	83 ± 25	1.43 ± 0.45
^{192}Ir (I)	11.4 ± 1.1	3.5 ± 0.6	3.26 ± 0.64
^{191}Au	7.8 ± 1.0 (R)	8.9 ± 1.1 (R)	0.88 ± 0.16
^{191}Pt	163 ± 7	152 ± 5	1.07 ± 0.06
^{190}Ir (I)	18.6 ± 1.5	6.9 ± 0.6	2.70 ± 0.32
^{189}Ir	151 ± 8	132 ± 5	1.14 ± 0.07
^{188}Pt	145 ± 7	136 ± 8	1.07 ± 0.08
^{188}Ir (I)	62 ± 15	25 ± 10	2.48 ± 1.16
^{186}Pt	51 ± 4 (R)	63 ± 3 (R)	0.81 ± 0.07
^{186}Ir^m	96 ± 10	74 ± 8	1.30 ± 0.20
^{185}Ir	109 ± 11	104 ± 10	1.05 ± 0.15
^{185}Os	139 ± 4	118 ± 3	1.18 ± 0.05
^{184}Ir	104 ± 3	102 ± 2	1.02 ± 0.04
^{183}Os	68 ± 14	55 ± 11	1.24 ± 0.36
^{183}Os^m	61 ± 3	62 ± 2	0.98 ± 0.06
^{183}Re	121 ± 4	99 ± 3	1.22 ± 0.05
^{182}Os	105 ± 5	94 ± 6	1.12 ± 0.09
^{181}Re	127 ± 6	104 ± 4	1.22 ± 0.07
^{177}Ta	46 ± 9	41 ± 8	1.12 ± 0.31
^{176}W	54 ± 6	49 ± 5	1.10 ± 0.17
^{175}Ta	36.7 ± 3.7	30.2 ± 3.0	1.22 ± 0.17
^{175}Hf	33.6 ± 1.7	27.9 ± 0.6	1.20 ± 0.07
^{174}Ta	26.3 ± 2.6	25.4 ± 2.5	1.04 ± 0.15
^{173}Ta	11.9 ± 0.4	11.3 ± 0.4	1.05 ± 0.05
^{171}Lu	8.4 ± 1.3	8.4 ± 0.6	1.00 ± 0.17
^{167}Tm	4.3 ± 0.8	4.1 ± 0.6	1.05 ± 0.25
σ_{obs}	1918 ± 31	1562 ± 34	$\sigma^-_{obs}/\sigma^+_{obs} = 1.228$
$\langle \Delta A \rangle$	10.00	10.41	

cross sections of ^{190}Ir and ^{192}Ir are also partial, because the electron capture decay branch of the short-lived isomers of the former was not observed, nor was the decay of 241-y ^{192}Ir^m.

III. RESULTS

The results of these measurements are presented in Tables III–V, which give the formation cross sections with π^+ and π^- mesons for each nuclide at the three pion energies used. The error given for each cross section represents only the statistical counting error, which was obtained from a least-squares fit of the observed counting data for each γ-ray peak to a decay curve using the known half-life, or, when appropriate, to a two-component decay curve. These are the proper errors to use in estimating the errors for relative values of the cross section ratio, $\sigma(\pi^-)/\sigma(\pi^+)$ for the nuclides studied, since the uncertainties in γ-ray abundance and counting efficiency cancel out. The uncertainty of ~10% in the values of the monitor cross sections has the effect of moving all the cross sections up or down together and is of importance in estimating the error in the total reaction cross section. In addition, the latter value will include the estimated uncertainty of 3% in the detector efficiency calibration and the uncertainty in the correction for summing of coincident γ rays where appropriate.

The values reported for the nuclides ^{191}Au and ^{186}Pt in Tables III–V are only relative cross sections, since the absolute abundance of their γ rays in unknown. They were calculated by assuming a γ-ray abundance of 1.0, and may be converted to absolute cross sections by dividing

TABLE V. Cross sections from interactions of 300-MeV $\pi^{\pm}$ mesons with ^{197}Au. Independent yields are indicated by (I); others are cumulative. Relative cross sections are indicated by (R). Errors refer to counting statistics only.

Nuclides	$\sigma(\pi^-)$ (mb)	$\sigma(\pi^+)$ (mb)	$\sigma(\pi^-)/\sigma(\pi^+)$
^{196}Au (I)	107 ± 1	61.4 ± 1.2	1.74 ± 0.04
^{196}Au^m (I)	4.6 ± 0.9	3.0 ± 0.6	1.53 ± 0.43
^{194}Au (I)	56.5 ± 0.6	37.8 ± 0.8	1.49 ± 0.04
^{193}Hg^m (I)	<0.5	5.6 ± 0.5	<0.09
^{193}Au		37 ± 5	
^{192}Hg (I)	<1	13.2 ± 0.7	<0.08
^{192}Au (I)	57 ± 6	40 ± 12	1.43 ± 0.45
^{192}Ir (I)	5.2 ± 0.3	3.4 ± 0.4	1.53 ± 0.20
^{191}Au	4.5 ± 0.7 (R)	4.1 ± 0.4 (R)	1.10 ± 0.20
^{191}Pt	68 ± 2	79 ± 4	0.86 ± 0.05
^{190}Ir (I)	10.0 ± 0.3	6.4 ± 0.5	1.56 ± 0.13
^{189}Ir	75 ± 3	81 ± 4	0.93 ± 0.06
^{188}Pt	69 ± 4	86 ± 4	0.80 ± 0.06
^{188}Ir (I)	30 ± 7	18 ± 5	1.67 ± 0.61
^{186}Pt	33 ± 2 (R)	42 ± 2 (R)	0.79 ± 0.06
^{186}Ir^m	72 ± 7	57 ± 6	1.26 ± 0.18
^{185}Ir	74 ± 4	64 ± 3	1.16 ± 0.07
^{185}Os	90 ± 1	84 ± 2	1.07 ± 0.03
^{184}Ir	65.8 ± 1.3	72.6 ± 1.5	0.91 ± 0.03
^{183}Os	47 ± 9	39 ± 8	1.21 ± 0.34
^{183}Os^m	44 ± 2	45 ± 2	0.98 ± 0.06
^{183}Re	83 ± 2	77 ± 4	1.08 ± 0.06
^{182}Os	71 ± 2	69 ± 2	1.03 ± 0.04
^{181}Re	81 ± 3	80 ± 3	1.01 ± 0.05
^{177}Ta	44.5 ± 1.8	41.3 ± 2.1	1.08 ± 0.06
^{176}W	66.0 ± 2.0	56.0 ± 2.2	1.18 ± 0.06
^{175}Ta	54 ± 6	42 ± 7	1.29 ± 0.26
^{175}Hf	48.1 ± 0.7	39.5 ± 0.8	1.22 ± 0.03
^{174}Ta	30.6 ± 3.1	28.0 ± 4.1	1.09 ± 0.19
^{173}Ta	21.4 ± 1.0	23.1 ± 1.2	0.93 ± 0.06
^{171}Lu	24.6 ± 0.5	21.1 ± 1.1	1.17 ± 0.07
^{170}Hf	12.0 ± 1.8	11.7 ± 0.7	1.03 ± 0.17
^{169}Lu	13.0 ± 1.5	9.8 ± 1.5	1.33 ± 0.25
^{167}Tm	9.7 ± 0.5	9.0 ± 0.5	1.08 ± 0.08
σ_{obs}	1210 ± 15	1148 ± 19	$\sigma^-_{obs}/\sigma^+_{obs} = 1.054$
$\langle \Delta A \rangle$	12.31	12.37	

by I_γ when that quantity becomes known.

It is difficult to evaluate the precision of the absolute γ-ray abundances used, except by noting any nuclides whose measured cross sections are systematically higher or lower than expected from assuming a smooth variation with A. Using that criterion, it seems likely that none of the abundances used is in error by more than 20%.

The sum of all observed cross sections at each energy is given at the bottom of Tables III–V. In this sum, double counting was not done; for example, the cross section for an isobar such as ^{185}Ir was not included in the sum, since it is already included in the cumulative cross section of ^{185}Os. In addition, the ratio of these sums for π^- and π^+ at each energy are given. The total observed cross section is quite large, especially at 180 MeV, and represents a major fraction of the reaction cross section. The method used for estimating the missing isobaric cross sections, and thus the total reaction cross section, will be described in the following section. The weighted average mass loss, $\langle \Delta A \rangle$, calculated from the observed cross sections is also given at the bottom of these tables. A better estimate of $\langle \Delta A \rangle$ is calculated using the smooth mass-yield curve for each energy and pion charge in the following section.

An overall view of the pattern of cross sections can be seen in Fig. 1, which shows the relevant portion of a Z vs N chart of the nuclides, showing the cross sections for the case of 180 MeV π^+.

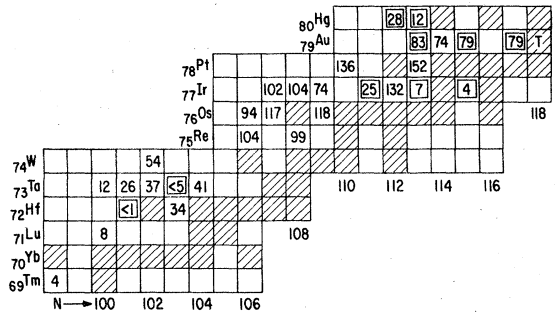

FIG. 1. Formation cross sections in mb for nuclides formed by bombardment of ^{197}Au with 180-MeV π^+ mesons as a function of Z and N. Numbers enclosed in squares denote independent cross sections; others are cumulative. Shaded nuclides are stable or long-lived. T = target.

The numbers within an inner box in the squares represent independent yields, and those in open squares represent cumulative yields. Stable or long-lived nuclides are indicated by shaded squares. The low independent cross sections observed for the heaviest iridium isotopes show that the peak of the charge dispersion curve near $A = 190$ is between Pt and Au. Also, one can note the approximate equality of cumulative cross sections for ^{185}Ir and ^{185}Os, for ^{183}Os^{m+g} and ^{183}Re, and for ^{175}Ta and ^{175}Hf, all demonstrating that these nuclides are far enough from the peak of the yield that they cumulate all of the isobaric yield. The small magnitude of the independent cross sections for ^{176}Ta and ^{173}Hf also shows this.

The pattern is very similar for π^-, with the exception that the peak yields are shifted somewhat to more neutron-excess nuclides. This is clearly seen in the cross section ratios $\sigma(\pi^-)/\sigma(\pi^+)$ for the shielded isotopes of iridium (Tables III–V) which are considerably larger than the average for all nuclides. This shift in peak yield is also obvious when one considers that, whereas Hg isotopes are formed with sizeable cross sections by π^+, they are not formed at all by π^-. This shift is largest close to the target, and has disappeared at a mass loss $\Delta A \approx 20$, as shown by the small independent cross section of ^{176}Ta and ^{173}Hf for both π^- and π^+.

The lightest nuclide observed in these experiments was ^{167}Tm, corresponding to a mass loss of 30 nucleons from the target. The fact that this nuclide is formed with a cross section of several mb at 100 MeV demonstrates the effectiveness of pion absorption in depositing excitation energy in the nucleus. Still lighter nuclides must be also formed, but with cross sections too small to be observed by the present technique. For example,

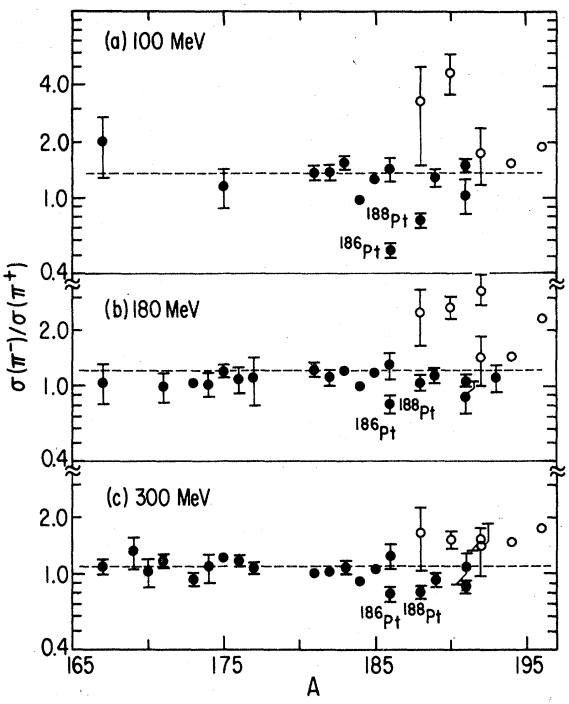

FIG. 2. Ratios of cross sections for forming specific nuclides by π^- and π^+ mesons at three energies. Open symbols indicate independent cross sections, solid symbols cumulative cross sections. The dashed line at each energy indicates the overall average ratio.

the formation of ^{24}Na from ^{197}Au by 176 MeV π^+ has been observed,[32] with a cross section of $\sim 10^{-2}$ mb.

The ratios of the cross sections for forming each nuclide by incident π^- and π^+ mesons, $\sigma(\pi^-)/\sigma(\pi^+)$, are shown in Fig. 2 for each energy as a function of nuclide mass number. The horizontal dashed lines indicate the overall ratio at each energy from the summed cross sections, as given at the bottom of Tables III–V. Nuclides for which independent cross sections were measured are shown as open symbols, and those for which cumulative cross sections were measured as solid symbols. The error bars represent only the errors due to the counting statistics and decay curve analysis, since errors in detector efficiency and γ-ray abundance cancel, and errors in the monitor cross sections result in a uniform shift in scale. The striking feature about these ratios is their near constancy as a function of A for the cumulative nuclides. Since such cumulative yields effectively integrate the isobaric yields, this constancy indicates that the *shape* of the mass yield curves are essentially identical for π^- and π^+ mesons of the same energy.

The magnitude of the ratios for nuclides whose

independent cross sections were measured (open symbols in Fig. 2) deviates significantly from the average, in the direction of larger $\sigma(\pi^-)$. In the case of the iridium isotopes, this is simply due to the shift in the most probable Z at a given A for π^- to a lower Z than for π^+, and to the location of these nuclides on the neutron-excess wing of the charge-dispersion curve. In the case of ^{196}Au, which is the product of the $(\pi, \pi N)$ reaction, the effect of the free-particle pion-nucleon cross sections is being seen, although in a reduced manner.[23] In the case of ^{194}Au and ^{192}Au one is probably seeing a similar sensitivity to the shift in the charge dispersion curve as for the iridium isotope.

The opposite deviation of the ratios is seen for ^{188}Pt and ^{186}Pt, especially at 100 MeV. The effect here is the same as that for the iridium isotopes, but on the other (neutron deficient) wing of the charge dispersion curve. For example, if one sees a larger ratio than average for ^{188}Ir, one should see a smaller ratio for ^{188}Pt, to the extent that the ^{188}Pt cumulative cross section from π^- is depleted.

The average π^-/π^+ cross section ratio is greater than unity, and decreases with increasing pion energy. This qualitative behavior is what one expects from Coulomb effects, since the π^- is attracted and the π^+ repelled by the nuclear Coulomb field. As discussed in the Introduction, there may also be isospin effects due to the large N/Z ratio of the target, whereby the probabilities of pion scattering and absorption might differ for positive and negative pions. Since scattering would be enhanced for negative pions and absorption enhanced for positive pions, the effect would be that the $\sigma(\pi^-)/\sigma(\pi^+)$ ratio would be smaller for nuclides with large ΔA than for nuclides close to the target. No such trend is seen in Fig. 2, suggesting that such isospin effects are of little significance.

The Coulomb effect may be estimated by the equation[33]

$$\frac{\sigma(\pi^-)}{\sigma(\pi^+)} = \frac{1+V/E_\pi}{1-V/E_\pi}. \tag{5}$$

In this equation $V = Ze^2/R$, Z is the nuclear charge, R the nuclear radius, and E_π the pion kinetic energy. For $R = 1.4A^{1/3}$, $V = 13.9$ MeV for ^{197}Au, we calculate values for $\sigma(\pi^-)/\sigma(\pi^+)$ of 1.32, 1.17, and 1.10 at energies of 100, 180, and 300 MeV, respectively. These agree quite well with the experimental ratios of 1.34, 1.23, and 1.05. We may therefore conclude that the differences in cross sections between π^- and π^+ projectiles are due almost entirely to the Coulomb effect, with little or no evidence of any isospin effects.

IV. DISCUSSION

A. Cascade-evaporation calculations

The results presented in the previous section can best be discussed in conjunction with a specific model for pion-nucleus reactions, the intranuclear cascade (INC) model, followed by an evaporation calculation. We obtained the computer codes for two INC calculations, the VEGAS-ISOBAR program[33-35] and the MECC-7 program,[36] and performed sample calculations with both. Comparisons showed that the results of the two calculations were very similar, indicating that the particular details of each code were not significantly influencing the results. The models are similar, in that the pion-nucleus interaction is described by sequential two-body scatterings of pions and nucleons in the nucleus. In the VEGAS-ISOBAR model a pion-nucleon interaction results in the creation of a Δ isobar, which may then interact with further nucleons or decay into a pion and nucleon. Pion absorption is treated as a two-body interaction of a Δ and a nucleon in which two nucleons result. In the MECC-7 model, pions are assumed to be absorbed on nucleon-nucleon pairs. Both models approximate the nuclear density distribution by a series of spherical shells of decreasing density, corresponding to the charge distributions obtained from electron scattering.

As a result of the intranuclear cascade, several particles are emitted and an excited residual nucleus remains, whose de-excitation is then calculated using statistical evaporation theory.[37] A level-density parameter of $a = A/10$ was used; since the nuclides of interest are far from closed shells, a smooth dependence of level density on mass number is reasonable. The calculated results discussed below are those of the VEGAS-ISOBAR code, in which the following options were chosen: (1) reflection and refraction of particles at the boundaries between density shells or at the nuclear surface was not used, (2) the pion-nucleus potential was taken to be zero, and (3) Δ-nucleon charge-exchange scattering was not allowed. At a single pion energy (180 MeV π^-) these options were varied to see what their effect would be, and the results will be discussed below. About 8000 interactions were computed for each case, and 10 evaporation chains were computed for each INC event, in order to decrease the statistical uncertainties. Comparisons of the experimental formation cross sections with the calculations are presented throughout the remainder of this section.

B. Cross section dependence on product mass

The distributions of the formation cross sections as a function of product mass number, $\sigma(A)$, are

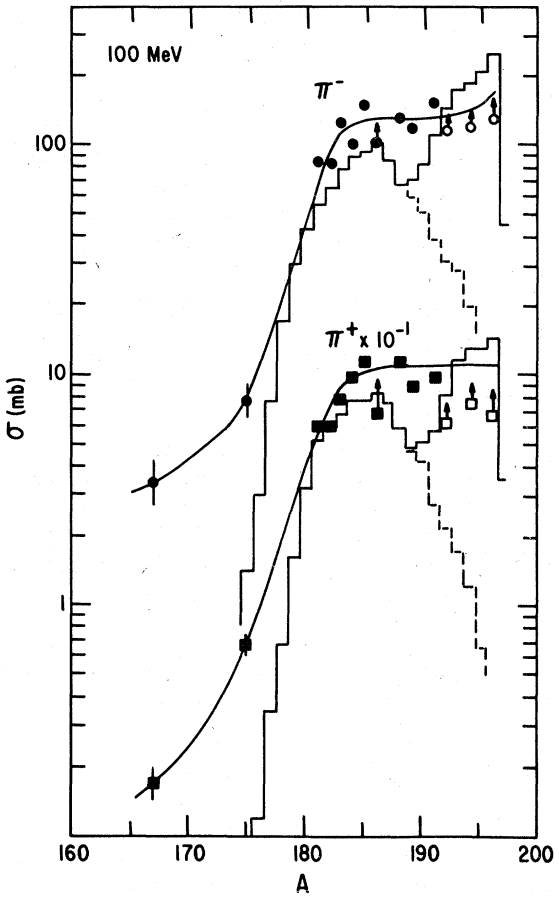

FIG. 3. Formation cross sections at 100 MeV. Open symbols indicate independent cross sections, solid symbols cumulative. Arrows denote partial isobaric yields. The histograms show the calculated $\sigma(A)$ from the INC model discussed in the text, with the dashed histogram showing the portion of the cross section due to pion absorption in the near-target region. The smooth curves represent our estimate of the smooth mass-yield curve. The π^+ data are offset by a factor of 10.

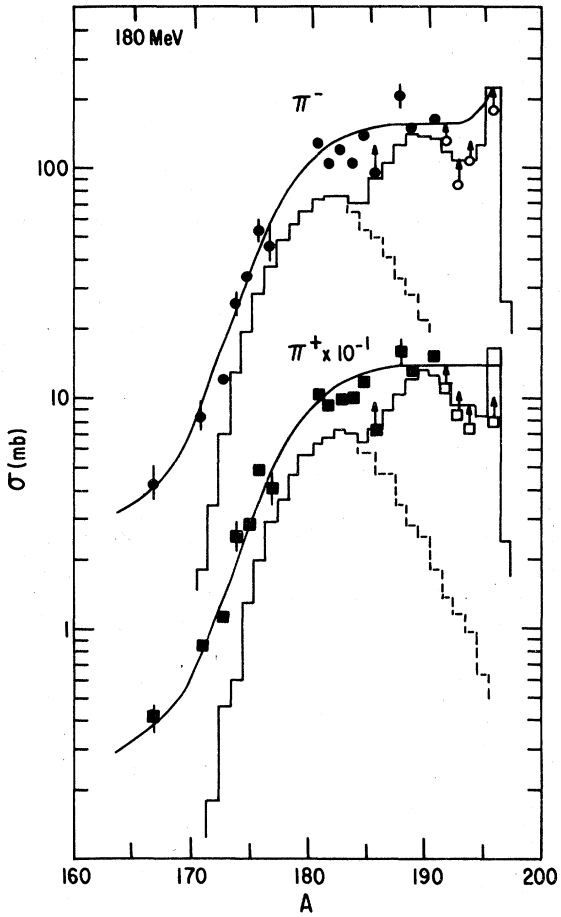

FIG. 4. Formation cross sections at 180 MeV. See caption to Fig. 3.

shown in Figs. 3–5. The π^- and π^+ data at each energy are shown in the same figure, with the π^+ data offset by a factor of ten, so that the shapes of the distributions may be easily compared. In each of these figures independent cross sections are indicated by open symbols and cumulative cross sections by closed symbols; thus the closed symbols represent the experimental values of $\sigma(A)$, the total isobaric cross section. In the case of cumulative cross section measurements on more than one isobar of a given mass number, the "most" cumulative is plotted; thus the value for ^{185}Os is shown, rather than ^{185}Ir. For mass numbers where both cumulative and independent cross sections were measured, such as ^{188}Pt and ^{188}Ir, their sum is plotted. A vertical arrow on a data point indicates that an appreciable fraction of the isobaric cross section was not measured, either because of stable products ($A = 192–196$) or because one isomer was not measured ($A = 186$).

The histograms in Figs. 3–5 show the calculated isobaric cross section at each mass number from the INC-evaporation calculation described above. The final nuclides after the evaporation were sorted according to whether the incident pion was absorbed or was scattered and eventually re-emitted (including charge exchange in the latter category). The solid histograms show the product distributions for all events, while the dashed portion shows the part arising from pion absorption for nuclides closer to the target. The contribution of scattering has fallen to zero where the dashed and solid histograms meet.

The cross section normalization in the calculations is absolute, in the following sense. The geometric cross section is given by $\sigma_g = \pi R_0^2$, where R_0 is the radius of the outermost shell in the assumed nuclear density distribution used in the model. If the fraction of events in which no

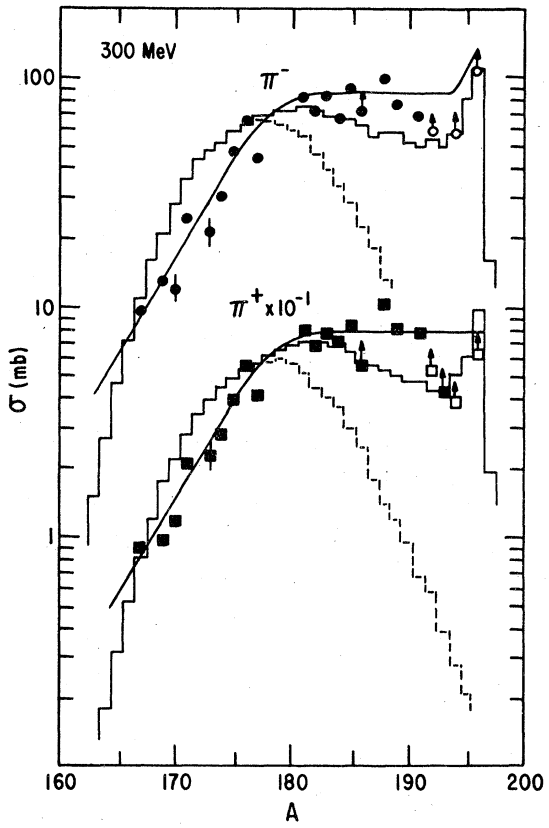

FIG. 5. Formation cross sections at 300 MeV. See caption to Fig. 3.

interaction occurred (transparencies) is t, and the Coulomb barrier is $V = Z_1 Z_2 e^2 / R_0$, then the reaction cross section is[33]

$$\sigma_r = \sigma_g (1 - t)(1 - V/E_p) , \quad (6)$$

where E_p is the kinetic energy of the projectile.

The smooth curves in Figs. 3–5 are our best estimates of the trend of the $\sigma(A)$ function, which is used to interpolate unmeasured cross sections to calculate the total reaction cross section (following section).

Comparing the experimental cross sections and the results of the calculations for 100 MeV $\pi^{\pm}$, shown in Fig. 3, one notes several things. The calculation underestimates the magnitude of the cross sections for products with $A < 192$. In particular, the largest mass loss calculated is $\Delta A = 22$, while we observe the nuclide ^{167}Tm ($\Delta A = 30$) with cross sections of 2–3 mb. Moreover, the calculation predicts a mass distribution with two distinct peaks, one due to scattering and the other to absorption. The experimental data show no indication of such behavior, but as shown by the smooth curve, are nearly constant in the region of the predicted dip. As indicated by the open symbols with arrows, the measurements of products close to the target ($A = 196, 194, 192$) do not cumulate the entire isobaric cross section. The missing yield is in the stable isotopes of Pt which are not detected.

Thus one cannot definitely state that the calculation overestimates the cross sections for $192 \leq A \leq 197$, although it would appear so, especially at $A = 196$. The calculated isobaric cross section at $A = 196$ for both π^- and π^+ is about twice the ^{196}Au cross section, and one would not expect equal cross sections for ^{196}Pt and ^{196}Au, because of the suppression of proton emission by the Coulomb barrier.

Summarizing the above observations, one can say that at 100 MeV the calculation underestimates the cross section for pion absorption (products far from target) and may overestimate that for pion scattering (products close to target). It is not clear if the failure to predict large enough mass loss is a defect in the INC portion or the evaporation portion of the calculation. Preequilibrium emission of one or more clusters (alpha particles, etc.) can be effective in leading to lighter products, but such a mechanism is not included in the INC calculation. Statistical evaporation of He ions is included in the evaporation part, but is not very probable for these nuclides at the excitation energies involved here.

The comparison between experiment and calculation at 180 MeV (Fig. 4) shows similar discrepancies. Again, the calculation does not result in any nuclei with ΔA as large as 30, and underestimates all cross sections in the mass region for which $\Delta A > 10$. At this energy it appears that products close to the target may not be overestimated, since the calculation is rather close to the incomplete isobaric cross section values. The general conclusion remains that pion absorption, and in fact the total reaction cross section, are underestimated by the INC model.

Turning to Fig. 5, which compares experiment and calculation at 300 MeV, one sees a different picture. The overall agreement is better over the entire range of products. The cross sections are somewhat underestimated in the $A = 185$–192 region, and are correspondingly overestimated for large ΔA, $A = 169$–175. What is probably happening is that the INC model gets better when the pion kinetic energy is larger than its rest mass and is above the (3, 3) resonance. Under those conditions the distinguishing features between pions and protons tend to vanish, and it is known[33] that the INC model accounts for proton reactions quite well.

Several options in the INC model are available, and these were varied in order to note the effect

on the final product distribution. One such option[34] is whether isobar-nucleon exchange scattering,

$$\Delta + N \rightarrow \Delta' + N', \tag{7}$$

is allowed, where Δ' and N' may have different charge than Δ and N, as well as different energy. Including this process in the calculation, at an energy of 180 MeV, did not affect the final mass and charge distributions at all.

Another option is whether refraction and reflection of the cascade particles at the boundaries between different density shells is permitted. This option was included, along with a distance restriction[38] on collisions to forbid successive collisions happening within one nucleon radius, taken to be $r = (4\pi\rho/3)^{-1/3}$, where ρ is the local nucleon density. The effect of this change, for both π^- and π^+ at 180 MeV, was to increase the contribution of scattering by about 40%, at the expense of absorption, with the total reaction cross section remaining the same. The mass-yield distribution thus is higher close to the target and lower at large ΔA, and thus is in poorer agreement with the data than when reflection and refraction are ignored.

C. Total reaction cross sections

A useful result of cross section measurements for a heavy target element would be an estimate of the reaction cross section, since that quantity is difficult to measure directly, owing to the large Coulomb scattering correction. If an empirical isobaric cross-section curve for $\sigma(A)$ can be constructed, the cross sections for unmeasured nuclides could then be estimated by interpolation. In constructing such a curve, theoretical guidance such as from the INC calculations, would be helpful, but it is clear from the comparisons in Figs. 3–5 that the results of these calculations are not a very accurate guide.

The smooth curves shown in Figs. 3–5 represent our best estimate of the variation of total isobaric cross section with mass number. In the region where the measured cross sections cumulate $>90\%$ of the isobaric yield, $A \lesssim 185$, the curves simply follow the trend of the data. Closer to the target, however, the measured cross sections probably represent a smaller fraction of the isobaric cross sections, and the exact shape of the curve is difficult to estimate. We have assumed a flat dependence on A near to the target, somewhat arbitrarily, and drawn the curve such that it lies above all of the partical cross sections (open symbols).

Using these smooth curves we estimated cross sections at those mass numbers for which no product was measured, and summed them to obtain σ_{interp}, the "interpolated" cross section. The second contribution to the total cross section which must be estimated is that due to isobars of measured nuclides which are not cumulated (symbols with vertical arrows in Figs. 3–5). The difference between the $\sigma(A)$ from the smooth curve and the measured cross sections of those nuclides are summed to obtain σ_{missing}, the "missing" cross section. Adding these two estimates to the total observed cross section, σ_{obs}, we obtain the total reaction cross section, σ_r. These quantities are given in Table VI for each energy and pion charge.

It is difficult to estimate the uncertainty in these cross sections. The values of σ_{obs} have as their main source of error the estimated uncertainty of $\sim 20\%$ due to poorly determined absolute γ-ray abundances. The errors in counting efficiency and the coincidence summing correction are much smaller. We will arbitrarily set the uncertainty in the values of σ_{interp} and σ_{missing} to 50%, which we feel is probably a conservative value. Combining these two uncertainties in quadrature, we obtain the errors on σ_r given in Table VI. Since all cross sections are dependent on the value of the monitor cross sections, the 10% uncertainty in those must be regarded as possible systematic

TABLE VI. Estimates of total reaction cross sections for pions on gold. Contributions to total are the sum of observed cross sections (σ_{obs}), interpolated (σ_{interp}), and correction for missing isobaric cross sections (σ_{missing}). The calculated reaction cross sections from the INC calculation are also given.

Beam energy (MeV)	Pion charge	σ_{obs} (mb)	σ_{interp} (mb)	σ_{missing} (mb)	σ_r (mb)	σ_r (calc) (mb)
100	−	1421	554	167	2142 ± 455	1997
100	+	1058	355	327	1740 ± 402	1404
180	−	1918	618	326	2862 ± 608	2077
180	+	1562	538	401	2501 ± 564	1772
300	−	1210	522	117	1849 ± 401	1713
300	+	1148	398	218	1764 ± 384	1554

errors in the values of σ_r.

Although the large uncertainties in σ_r appear to make any use of these numbers of little value, that is not strictly so. The errors involved in these estimates are not random, since the same γ-ray abundances and counting efficiencies are used in each case. Furthermore, the smooth curves used for interpolation are of similar shapes, so that the relative magnitudes of the estimated σ_r are better determined than indicated by the errors given.

With these considerations in mind, we make the following observations. The effect of the (3, 3) resonance is clearly seen as a maximum in σ_r at 180 MeV for both π^- and π^+, and in both the experimental estimate and the INC calculation. The INC-calculated reaction cross section is close to the "experimental" σ_r for 100 MeV π^- and 300 MeV π^- and π^+. For both pion charges at 180 MeV, the INC result is significantly smaller than the experimental estimate. This is an indication that a heavy nucleus such as ^{197}Au interacts more strongly with pions near the peak of the (3, 3) resonance than would be predicted. The "missing" cross section in the calculation appears to be due to pion absorption, as discussed in the previous section. A better estimate of σ_r than obtained here would require (1) better information on decay schemes of the nuclides measured, and (2) measurement of additional nuclides, especially non-radioactive nuclides close to the target. The latter could be done by an in-beam prompt γ-ray experiment.

An indirect way to get better estimates of such cross sections is the use of charge dispersion curves, i.e., the variation of independent cross section with Z at a given A. Knowledge of the shape of such curves for a number of A values would allow one to estimate the fraction of the total $\sigma(A)$ which was not measured due to stable nuclides. Unfortunately, there are too few independent yields measured in this work to permit us to construct such curves. Even at $A = 192$ for π^+ mesons, where three independent yields were determined at 180 and 300 MeV, that for ^{192}Ir is only a lower limit, because the contribution of 240-y ^{192}Ir^m was not measured.

E. Excitation functions

Although cross section measurements at only three energies do not constitute a complete excitation function, they nevertheless provide an outline of one. In presenting these excitation functions we have removed the dependence of the total reaction cross section, σ_r, on pion charge and kinetic energy (Table VI) by plotting the ratio σ/σ_r, using our estimated experimental σ_r values. The excitation functions for several types of products are shown in Fig. 6, where solid symbols refer to π^- reactions and open symbols to π^+ reactions.

The results for three nuclides close to the target, ^{194}Au, ^{193}Hg^m, and ^{192}Hg, are shown in Fig. 6(a). They all show a similar behavior, with decreasing cross sections. The similarity between the π^- and π^+ excitation functions for ^{194}Au is clearly shown. Since the nuclear charge cannot be increased in the π^- bombardment, mercury isotopes are not formed. However, the excitation functions of ^{193}Hg^m and ^{192}Hg for incident π^+ mesons are similar to those for ^{194}Au. Formation of these near-target nuclides is due to interactions where relatively small amounts of excitation energy are transferred to the nucleus. Thus, one expects that the probability of their formation should decrease as the available energy increases.

The excitation functions for three nuclides farther removed from the target, ^{185}Os, ^{182}Os, and ^{175}Hf, are shown in Fig. 6(b). The cross sections for these nuclides, normalized to σ_r, are virtually identical for incident π^- and π^+ mesons. The shapes of their excitation functions illustrate the changes as the product mass number decreases. The ^{185}Os cross section decreases between 100 and 180 MeV, and then remains constant up to 300 MeV. The ^{182}Os cross section is nearly the same at all three energies, while a nuclide far removed from the target, such as ^{175}Hf, shows a sharply increasing excitation function, indicating the large deposition energies required for its formation.

The similarity between the π^- and π^+ cross sections, once the total reaction cross section is factored out, shows again the nearly isospin independence of these processes. The main difference between the interactions of the two pion charge states and a heavy nucleus is simply due to Coulomb effects, rather than any specific pion-nucleus interaction.

F. Comparison with stopped pion measurements

It is instructive to compare the present data with similar measurements[21] of the products formed when stopped negative pions are absorbed by a heavy nucleus. Since ^{197}Au was one of the targets used in those measurements, a direct comparison of product nuclides can be done. In the stopped-pion experiment[21] both prompt and delayed γ rays were measured, allowing determination of the yields of stable as well as radioactive nuclides. The major fraction of the yield, about 74%, was found as isotopes of Pt, and the remainder as

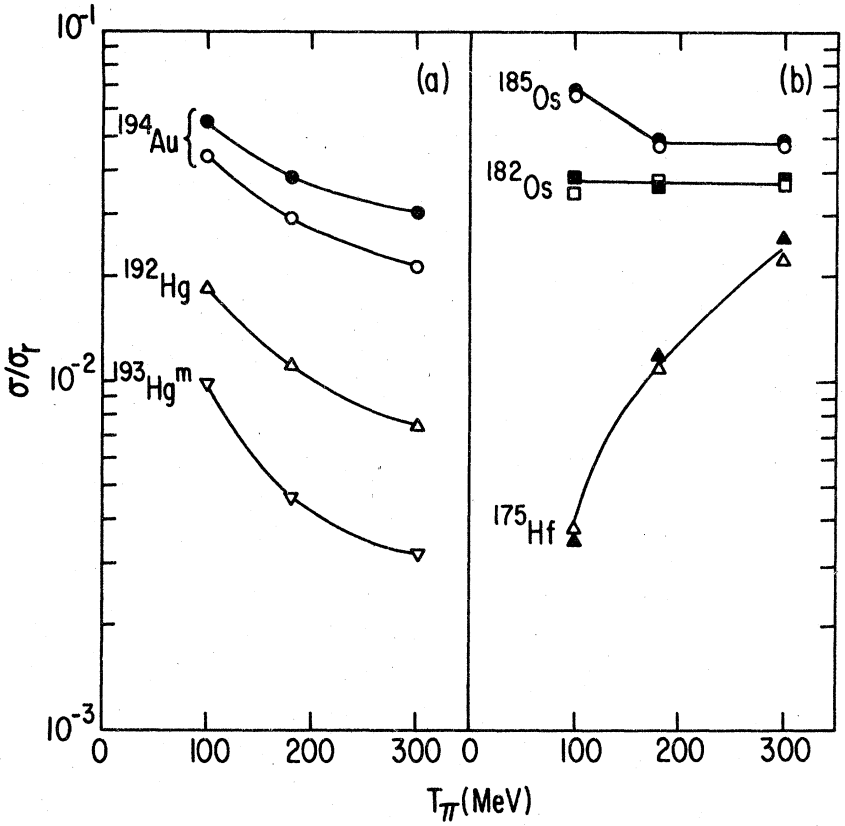

FIG. 6. Excitation functions for typical nuclides formed by $\pi^{\pm}$ mesons on gold. The cross sections have been normalized to the total reaction cross sections at each energy, given in Table V. Open symbols are π^+ data, solid symbols π^-.

isotopes of Ir. No isotopes of Au are formed, because absorption of the π^- decreases the atomic number by one, and the Coulomb barrier suppresses emission of more than one charged particle, so elements of lower Z than 77 are not formed as primary products.

We have used the data of Pruys *et al.*,[21] to construct a mass-yield curve for stopped pions in ^{197}Au, and it is shown as the solid curve in Fig. 7. The mass-yield curves at π^- kinetic energies of 100, 180, and 300 MeV, taken from Figs. 3–5, are also shown in Fig. 7 for comparison. All curves are shown as fractional yields, using the values of σ_r at each kinetic energy to calculate the fractional yields.

The effect on the mass-yield curve of increasing the pion kinetic energy from 0 MeV to 300 MeV is clearly shown in Fig. 7. The average mass lost from the target increases with increasing energy, and the slope of the curve as it falls off decreases, so that larger mass losses become more probable. Thus, for example, the mass loss for which the yield has fallen to the 1% level increases from $\Delta A = 13$ for stopped pions to $\Delta A = 19$, 23, and 26

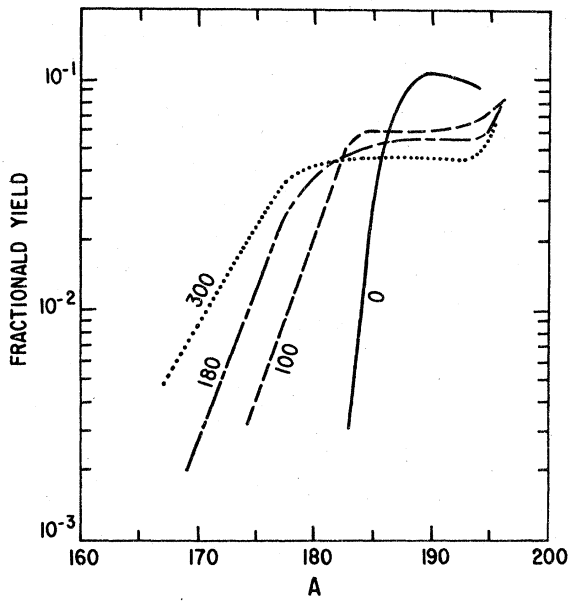

FIG. 7. Smooth mass-yield curves, relative to the total reaction cross section, for stopped pions (Ref. 21) and for 100–300 MeV pions.

at energies of 100, 180, and 300 MeV. The average mass loss calculated from the mass yield curves is $\langle \Delta A \rangle = 6.9$, 8.5, 10.0, and 11.6 in order of increasing energy.

This distinct increase in the amount of excitation energy transferred to the nucleus is in contrast to the results on nickel targets[13] where the average numbers of neutrons and protons lost were nearly independent of pion kinetic energy. However, a similar increase in mean excitation with increasing pion kinetic energy was deduced[16] for the spallation of copper.

An interesting phenomenon which was noted[17,20-22] in the absorption of stopped negative pions is the production of relatively high spin states in the products. This was explained as being due to absorption on a quasideuteron near the nuclear surface and the escape of one fast neutron and the absorption of the other. The kinematics of this process then leads to similar angular momenta as would result from ~70-MeV neutrons interacting at large impact parameters. Only four isomeric states were observed in the present work; two of those ($^{186}Ir^m$ and $^{183}Os^m$) are formed largely by electron capture decay of their radioactive parents, rather than directly. In the case of $^{193}Hg^m$ we cannot determine an isomeric ratio, since the ground state was not detected. Only for $^{196}Au^m$ is this possible; the isomeric ratio $\sigma(12-)/\sigma(2-)$ is quite small for pions of 100–300 MeV, varying between 0.03–0.06. However, it is clear that pion absorption is not involved in forming ^{196}Au, but rather pion scattering, for which one expects little angular momentum to be imparted. Therefore, the low isomeric ratio for this nuclide is understandable, and should not be compared with the higher ratios observed for stopped pions.

V. CONCLUSIONS

As a result of the data presented and discussed above, we may make the following conclusions about the interaction of pions with a heavy nucleus in the region of the (3, 3) resonance:

(1) The most probable yield for a given mass does not fall near the beta-stability line, but tends to be several charge units toward the neutron-poor region. As a result, most of the observed nuclides are not the primary products but are formed largely after several electron-capture decays of their precursor isobars. In the few cases where primary products were observed (independent yields) they show that the displacement of yield toward the neutron-poor nuclides is larger for positive pions than for negative pions, especially for nuclides near the target. This is probably not the result of pion absorption transferring the pion charge, but rather to charge exchange reactions of the type $(\pi^{\pm}, \pi^0 xn)$.

(2) The cross sections resulting from negative pion bombardment are larger than those from positive pions; the average ratios at 100, 180, and 300 MeV are 1.34, 1.23, and 1.05, respectively. These ratios are close to those expected from the effect of the Coulomb field of the nucleus, showing that the pion-nucleus interactions are the same, and are not distorted by isospin effects associated with the large neutron-excess of the target. At a given energy the ratio is nearly independent of mass number, indicating that the shape of the mass-yield curve is the same for incident π^- and π^+ mesons.

(3) The total reaction cross section, estimated by interpolation for unmeasured nuclides, has a maximum near 180 MeV, reflecting the influence of the (3, 3) pion-nucleon resonance. At 180 MeV the estimated experimental reaction cross section is significantly larger than that calculated from an intranuclear cascade (INC) calculation.

(4) The INC calculation appears to predict less pion absorption than actually occurs. This is shown both by a deficiency in the calculated yield in the mass region $A = 180$–190, and by the failure of the calculation to predict appreciable yields of nuclides far from the target. The INC calculation is in better agreement with experiment at 300 MeV than at the lower energies.

(5) The average excitation energy transferred to the nucleus is similar for positive and negative pions, and increases with increasing pion kinetic energy. This is shown by the comparative mass-yield curves for stopped pions and the three energies of the present work. Moreover, the distribution of excitation energy, as indicated by the mass-yield curves, are similar for π^+ and π^- mesons.

ACKNOWLEDGMENTS

We wish to acknowledge the assistance of D. G. Perry in the early phase of this work. We are grateful to B. J. Dropesky and the LAMPF Nuclear Chemistry group for their hospitality. J. N. Ginocchio provided the FORTRAN program for the most recent version of the VEGAS INC calculation. This research was supported by the Division of Nuclear Physics of the U. S. Department of Energy.

[1]H. E. Jackson, L. Meyer-Schützmeister, T. P. Wangler, R. P. Redwine, R. E. Segel, J. Tonn, and J. P. Schiffer, Phys. Rev. Lett. 31, 1353 (1973).
[2]V. G. Lind, H. S. Plendl, H. O. Funsten, W. J. Kossler, B. J. Lieb, W. F. Lankford, and A. J. Buffa, Phys. Rev. Lett. 32, 479 (1974).
[3]D. Ashery, M. Zaider, Y. Shamai, S. Cochavi, M. A. Moinester, A. I. Yavin, and J. Alster, Phys. Rev. Lett. 32, 943 (1974).
[4]H. Ullrich, E. T. Boschitz, H. D. Engelhardt, and C. W. Lewis, Phys. Rev. Lett. 33, 433 (1974).
[5]B. J. Lieb and H. O. Funsten, Phys. Rev. C 10, 1753 (1974).
[6]H. E. Jackson, D. G. Kovar, L. Meyer-Schützmeister, R. E. Segel, J. P. Schiffer, S. Vigdor, T. P. Wangler, R. L. Burman, D. M. Drake, P. A. M. Gram, R. P. Redwine, V. G. Lind, E. N. Hatch, O. H. Otteson, R. E. McAdams, B. C. Cook, and R. B. Clark, Phys. Rev. Lett. 35, 641 (1975); 35, 1170 (1975).
[7]R. E. Segel, L. R. Greenwood, P. Debevec, H. E. Jackson, D. G. Kovar, L. Meyer-Schützmeister, J. E. Monahan, F. J. D. Serduke, T.P. Wangler, W. R. Wharton, and B. Zeidman, Phys. Rev. C 13, 1566 (1976).
[8]B. J. Lieb, W. F. Lankford, S. H. Dam, H. S. Plendl, H. O. Funsten, W. J. Kossler, V. G. Lind, and A. J. Buffa, Phys. Rev. C 14, 1515 (1976).
[9]Y. Cassagnou, H. E. Jackson, J. Julien, R. Legrain, L. Roussel, S. Barbarino, and A. Palmeri, Phys. Rev. C 16, 741 (1977).
[10]M. Zaider, D. Ashery, S. Cochavi, S. Gilad, M. A. Moinester, Y. Shamai, and A. I. Yavin, Phys. Rev. C 16, 2313 (1977).
[11]R. Legrain, Y. Cassagnou, J. Dalmas, H. E. Jackson, J. Julien, L. Roussel, and A. Palmeri, Phys. Lett. 74B, 207 (1978).
[12]B. J. Lieb, H. O. Funsten, C. E. Stronach, H. S. Plendl, and V. G. Lind, Phys. Rev. C 18, 1368 (1978).
[13]H. E. Jackson, S. B. Kaufman, D. G. Kovar, L. Meyer-Schützmeister, K. E. Rehm, J. P. Schiffer, S. L. Tabor, S. E. Vigdor, T. P. Wangler, L. L. Rutledge, Jr., R. E. Segel, R. L. Burman, P. A. M. Gram, R. P. Redwine, and M. A. Yates-Williams, Phys. Rev. C 18, 2656 (1978).
[14]C. K. Garrett and A.L. Turkevich, Phys. Rev. C 8, 594 (1973).
[15]N. P. Jacob, Jr. and S. S. Markowitz, Phys. Rev. C 13, 754 (1976).
[16]C. J. Orth, B. J. Dropesky, R. A. Williams, G. C. Giesler, and J. Hudis, Phys. Rev. C 18, 1426 (1978).
[17]V. M. Abazov, S. R. Avramov, V. S. Butsev, E. P. Cherevatenko, D. Chultem, W. D. Fromm, Dz. Ganzorig, Yu. K. Gavrilov, and S. M. Polikanov, Nucl. Phys. A274, 463 (1976).
[18]H. S. Pruys, R. Hartmann, R. Engfer, U. Sennhauser, W. Dey, H.-J. Pfeiffer, H. K. Walter, J. Morgenstern, and A. Wyttenbach, Helv. Phys. Acta 50, 199 (1977).
[19]H. K. Walter, W. Dey, H.-J. Pfeiffer, U. Sennhauser, R. Engfer, R. Hartmann, E. A. Hermes, H. P. Isaak, H. Müller, H. S. Pruys, F. Schlepütz, J. Morgenstern, and A. Wyttenbach, Helv. Phys. Acta 50, 561 (1977).
[20]R. Beetz, F. W. N. de Boer, J. K. Panman, J. Konijn, P. Pavlopoulos, G. Tibell, K. Zioutas, I. Bergström, K. Fransson, L. Tauscher, P. Blüm, R. Guigas, H. Koch, H. Poth, and L. M. Simons, Z. Phys. A286, 215 (1978).
[21]H. S. Pruys, R. Engfer, R. Hartmann, U. Sennhauser, H.-J. Pfeiffer, H. K. Walter, J. Morgenstern, A. Wyttenbach, E. Gadioli, and E. Gadioli-Erba, Nucl. Phys. A316, 365 (1979).
[22]C. J. Orth, W. R. Daniels, B. J. Dropesky, R. A. Williams, G. C. Giesler, and J. N. Ginocchio, Phys. Rev. C (to be published).
[23]S. B. Kaufman, E. P. Steinberg, and G. W. Butler, Phys. Rev. C 20, 262 (1979).
[24]R. D. Werbeck and R. J. Macek, IEEE Trans. Nucl. Sci. 22, 1598 (1975).
[25]R. A. Williams, C. J. Orth, G. W. Butler, G. C. Giesler, M. A. Yates-Williams, and B. J. Dropesky (unpublished).
[26]R. Gunnink and J. B.Niday, UCRL Report No. 51061, 1972 (unpublished).
[27]J. T. Routti and S. G. Prussin, Nucl. Instrum. Methods 72, 125 (1969).
[28]Nuclear Data Sheets, 16–25 (1975–1978).
[29]W. W. Bowman and K. W. MacMurdo, At. Data Nucl. Data Tables 13, 89 (1974).
[30]G. Erdtmann and W. Soyka, J. Radioanal. Chem. 27, 137 (1975).
[31]G. J. McCallum and G. E. Coote, Nucl. Instrum. Methods 130, 189 (1975).
[32]N. T. Porile, B. J. Dropesky, and R. A. Williams, Phys. Rev. C 18, 2231 (1978).
[33]K. Chen, Z. Fraenkel, G. Friedlander, J. R. Grover, J. M. Miller, and Y. Shiamoto, Phys. Rev. 166, 949 (1968).
[34]G. D. Harp, K. Chen, G. Friedlander, Z. Fraenkel, and J. M. Miller, Phys. Rev. C 8, 581 (1973).
[35]J. N. Ginocchio, Phys. Rev. C 17, 195 (1978).
[36]H. W. Bertini, Phys. Rev. C 6, 631 (1972).
[37]I. Dostrovsky, Z. Fraenkel, and G. Friedlander, Phys. Rev. 116, 683 (1959).
[38]K. Chen, G. Friedlander, G. D. Harp, and J. M. Miller, Phys. Rev. C 4, 2234 (1971).